



1  
2  
3  
4  
5  
6  
7  
8  
9  
10  
11  
12  
13  
14  
15  
16  
17  
18  
19  
20  
21  
22  
23  
24  
25  
26  
27  
28  
29  
30  
31

*Geophysical Research Letters*

Supporting Information for

**Spatially resolved photochemistry impacts emissions estimates in fresh wildfire plumes**

**Brett B. Palm<sup>1,\*,#</sup>, Qiaoyun Peng<sup>1</sup>, Samuel R. Hall<sup>2</sup>, Kirk Ullmann<sup>2</sup>, Teresa L. Campos<sup>2</sup>, Andrew Weinheimer<sup>2</sup>, Deedee Montzka<sup>2</sup>, Geoffrey Tyndall<sup>2</sup>, Wade Permar<sup>3</sup>, Lu Hu<sup>3</sup>, Frank Flocke<sup>2</sup>, Emily V. Fischer<sup>4</sup>, Joel A. Thornton<sup>1</sup>**

<sup>1</sup>Department of Atmospheric Sciences, University of Washington, Seattle, WA, USA 98195

<sup>2</sup>Atmospheric Chemistry Observations and Modeling Laboratory, National Center for Atmospheric Research, Boulder, CO, USA 80301

<sup>3</sup>Department of Chemistry and Biochemistry, University of Montana, Missoula, MT, USA 59812

<sup>4</sup>Department of Atmospheric Science, Colorado State University, Fort Collins, CO, USA 80523

<sup>@</sup>Now at: Atmospheric Chemistry Observations and Modeling Laboratory, National Center for Atmospheric Research, Boulder, CO, USA 80301

<sup>#</sup>Corresponding author: Brett B. Palm (bbpalm@ucar.edu)

**Contents of this file**

- Text S1 to S4
- Figures S1 to S13
- Table S1

## 32 S1 Instrument and measurement details

33 The I<sup>-</sup> CIMS measured a variety of organic and inorganic compounds, including HONO,  
34 HCN, several likely phenolic compounds, and a suite of other oxidized organic compounds.  
35 Ambient air was sampled at 20 lpm through a 3/4" OD, ~50 cm long PTFE Teflon tube into the  
36 cabin. Air was then subsampled at 2 slpm into the CIMS through a custom inlet (Palm et al.,  
37 2019). Data was collected at 2 Hz and averaged to 1 Hz for use. The calibration factors used for  
38 each compound are described in Palm et al. (2020). C<sub>3</sub>H<sub>4</sub>O<sub>3</sub> was not calibrated due to a lack of  
39 knowledge of the sampled isomer composition, so mixing ratios were calculated using a typical  
40 calibration value of 5 counts per second per million reagent ions per pptv. C<sub>6</sub>H<sub>6</sub>O<sub>2</sub> was screened  
41 to remove measurement "tails" that result from that compound interacting with inlet surfaces  
42 (see Palm et al., 2019), by removing any C<sub>6</sub>H<sub>6</sub>O<sub>2</sub> data where C<sub>6</sub>H<sub>6</sub>O<sub>1</sub> (a compound with minimal  
43 inlet surface interactions) had decayed to below 20% of its peak in each transect. The other I<sup>-</sup>  
44 CIMS compounds used here are more volatile and thus did not have such inlet artifacts.

45 CO was sampled using a commercial Mini-QCL tunable diode laser infrared absorption  
46 spectrometer (Lebegue et al., 2016). To optimize measurement accuracy, the spectrometer  
47 optical bench was continuously purged with synthetic zero grade air from which CO had been  
48 scrubbed to contain less than 1 ppbv. N<sub>2</sub>O was also measured by the Mini-QCL, and was  
49 quantified in the purge gas at typically less than 0.3 ppbv. The N<sub>2</sub>O purge gas concentration was  
50 included in spectral fit calculations to better reproduce the spectral background. The CO  
51 measurement had a precision of 0.1 ppbv with a 2 s temporal resolution and an accuracy of +/-  
52 0.6 ppbv. The photolysis rate of HONO ( $j_{\text{HONO}}$ ) was calculated from actinic flux measurements  
53 taken by the HIAPER Atmospheric Radiation Package (HARP; Shetter & Müller, 1999). Ozone  
54 (O<sub>3</sub>) was measured by a chemiluminescence instrument at 1 Hz, with an accuracy of 5%. A  
55 proton transfer reaction time-of-flight mass spectrometer (PTR-ToF-MS) was used to measure a  
56 suite of volatile organic compounds (VOCs), including C<sub>6</sub>H<sub>6</sub> and C<sub>7</sub>H<sub>8</sub> used here (Permar et al.,  
57 2021). The data from various instruments were aligned in time by maximizing correlations of  
58 non-reactive compounds in the plumes.

59 The physical age of each transect was estimated by dividing the average distance from  
60 each transect to the fire source location by the average wind speed measured in the plume. The  
61 solar zenith angle (SZA) at time of emission (sampled time minus physical age) was calculated  
62 for each sampled latitude and longitude using the NOAA Solar Calculator, based on equations  
63 from *Astronomical Algorithms*, by Jean Meeus.

64 NEMRs were calculated as background-subtracted ratios of various compounds to CO.  
65 The background values were determined by averaging out-of-plume measurements from before  
66 and/or after each transect (typically 15 s on each side) to get a single background value per  
67 transect for each compound. Some transects did not fully exit the plume, so their background  
68 values were determined using data from only one side of the transect. Such transects were  
69 identified by comparing with the backgrounds determined in nearby transects and looking for  
70 outliers. While the South Sugarloaf fire was confined to (and diluted with) the boundary layer,  
71 the airplane occasionally transitioned into free tropospheric air while sampling the background  
72 before or after some transects sampled at the very top of the plume. Free tropospheric air was

73 identified by, e.g., low mixing ratios of water vapor, formic acid, and a variety of other  
74 compounds. This air was not representative of the air with which the plume was diluting, so such  
75 measurements were not included as background values. The Taylor Creek Fire plume, on the  
76 other hand, was injected into (and predominantly diluted with) the free troposphere, so  
77 background values were selected from free tropospheric air before and after each transect.

## 78 **S2 Methodology for estimating $[\text{OH}]_{\text{avg}}$ in the Taylor Creek Fire plume**

79 In non-diluting systems, e.g., batch chamber experiments of photochemical aging, OH  
80 concentrations can be derived by measuring the decay of a single compound and applying  
81 reaction kinetics. In diluting systems, e.g., urban downwind or wildfire plumes, the  
82 photochemical aging can be spatially inhomogeneous and difficult to estimate because of  
83 dilution and variations in parameters such as actinic flux. Previous studies of urban plumes have  
84 estimated photochemical age at various locations downwind by analyzing the change in the ratio  
85 of two compounds with a known emission ratio (de Gouw et al., 2005; Roberts et al., 1984).  
86 Dilution acts equally on the concentration of both compounds, so a change in the ratio indicates  
87 oxidation chemistry (or other formation/loss processes) when the two compounds have different  
88 reactivities. For systems where physical age can be estimated (e.g., wildfire or other point  
89 sources), the photochemical age estimated from changing ratios can be converted to average  
90 oxidant concentrations.

91 Past studies of urban air have used various organic compounds but not CO (de Gouw et  
92 al., 2005; Roberts et al., 1984), because CO is emitted by many urban sources at different rates.  
93 For wildfires, CO emissions can be characterized directly with measurements for individual fires,  
94 so it can be used as one of the two compounds.

95 To estimate the fractional fate of  $\text{C}_6\text{H}_6\text{O}_2$  to reaction with OH,  $\text{NO}_3$ , or  $\text{O}_3$  in the Taylor  
96 Creek Fire plume, we used the Framework for 0-D Atmospheric Modeling (F0AM) box model  
97 with the Master Chemical Mechanism (MCM) v3.3.1 chemical mechanism (Jenkin et al., 2015;  
98 Wolfe et al., 2016). The MCM is a near-explicit chemical mechanism with detailed gas-phase  
99 chemical processes for a variety of compounds, including 142 primarily emitted non-methane  
100 VOCs and their oxidation products. Additional mechanisms were added, including the recent  
101 mechanism development from laboratory measurements for heterocyclic hydrocarbons (like  
102 furans) and phenolics, which are found to significantly contribute to secondary product  
103 formation in biomass burning plumes (Coggon et al., 2019; Decker et al., 2019; Joo et al., 2019).

104 In Fig. S3, we show the fractional loss of  $\text{C}_6\text{H}_6\text{O}_2$  to each of the oxidants when  
105 initializing the model with mixing ratios measured in the core (95<sup>th</sup> percentile [CO]) or the edges  
106 (30<sup>th</sup> percentile [CO]) of the plume, along with production and loss rates of  $\text{C}_6\text{H}_6\text{O}_2$  as a function  
107 of plume age in the plume core. We estimate that 28% of  $\text{C}_6\text{H}_6\text{O}_2$  will react with  $\text{NO}_3$  in the core  
108 (roughly constant as a function of plume age), and 10% on the edges.  $\text{O}_3$  accounts for a  
109 negligible several percent, with the remainder going to reaction with OH. When estimating the  
110 fractional fates across the entire plume for the purposes of estimating  $[\text{OH}]_{\text{avg}}$  in Sect. 3.1.2, we  
111 assumed 75% of  $\text{C}_6\text{H}_6\text{O}_2$  reacted with OH in the Taylor Creek plume. The uncertainties  
112 associated with this assumption are likely small relative to those in the sensitivity analysis of the

113 initial  $C_6H_6O_2$  to CO ratio in Sect S3. This analysis also suggests that reaction with OH, not with  
114  $NO_3$ , was the cause of the measured crosswind gradients, since  $NO_3$  was found to account for  
115 less reaction on the edges versus the plume core. This estimation of the fractional fate of  $C_6H_6O_2$   
116 applies only to the Taylor Creek Fire plume, where the relatively bright midday plume  
117 conditions may have minimized the influence of  $NO_3$  chemistry.  $C_6H_6O_2$  may not be suitable for  
118 estimating [OH] in other plumes, particularly those emitted near or after sunset or in other  
119 conditions where non-OH chemistry is enhanced.

### 120 **S3 Sensitivity analysis**

121 Since it was not possible to sample the exact emission ratios of highly reactive  
122 compounds such as  $C_6H_6O_2$  in authentic wildfires from the aircraft platform, the initial ratio of  
123  $C_6H_6O_2$  to CO is a source of uncertainty. In Sect. 3.1.2, we used an initial ratio of 1. The  
124 evolution of this ratio with plume age is shown in Fig. S6b. In Fig. S5, we show the calculations  
125 of  $[OH]_{avg}$  using initial ratios of 0.7 and 1.5 to show the sensitivity of this calculation to the  
126 initial ratio. The estimated  $[OH]_{avg}$  in the freshest transects varies by up to approximately a factor  
127 of two, but the gradients are robust. The  $[OH]_{avg}$  in aged transects is less sensitive to the initial  
128 ratio. We also investigated the use of different compound ratios, including  $C_6H_6O_1$  to CO,  
129  $C_6H_6O_2$  to  $C_6H_6O_1$ , and  $C_7H_8$  to  $C_6H_6$  as shown in Fig. S6. None of the compounds except  
130  $C_6H_6O_2$  were expected to react appreciably with oxidants other than OH. The results were  
131 similar, with the exception that the fresh plume gradients were not as clear when  $C_6H_6O_2$  is not  
132 one of the compounds used. The likely reason for this behavior is that  $C_6H_6O_2$  is the only  
133 compound that reacts with OH fast enough to form measureable crosswind gradients on this time  
134 scale. After an estimated 22 min of physical age in the freshest transects, the fraction of  $C_6H_6O_2$   
135 remaining for  $[OH]_{avg}$  values of  $1.0 \times 10^7$  and  $4 \times 10^6$  molecules  $cm^{-3}$  (plume edges versus core)  
136 is expected to be 30% and 62%, which is a measurable difference in the freshest crosswind  
137 transects. For  $C_6H_6O_1$ , we expect 73% and 88% remaining, which is similar to the expected  
138 measurement precision and other possible uncertainties (e.g., any variable emissions between  
139 core and edge). For  $C_7H_8$ , 94% and 97% are expected, which are indistinguishable in a single  
140 crosswind transect to within uncertainties, and  $C_6H_6$  is even less reactive. Therefore,  $C_6H_6O_2$  was  
141 the best available compound for calculating  $[OH]_{avg}$  in the highly reactive and fresh Taylor  
142 Creek plume, and compounds such as  $C_7H_8$  and  $C_6H_6$  are not suitable for quantifying crosswind  
143 gradients on such short time scales. However, these slower-reacting compounds will still be  
144 useful for quantifying [OH] on the longer time scales of several hours or longer during  
145 downwind transport.

### 146 **S4 Additional vertically stacked transects in the South Sugarloaf fire**

147 Gradients can be observed by plotting NEMRs as a function of excess CO, where the  
148 densest part of the plume has the highest excess CO. An example is shown in Fig. S8 for a the  
149 second highest vertically stacked transect from Fig. 3/S9.

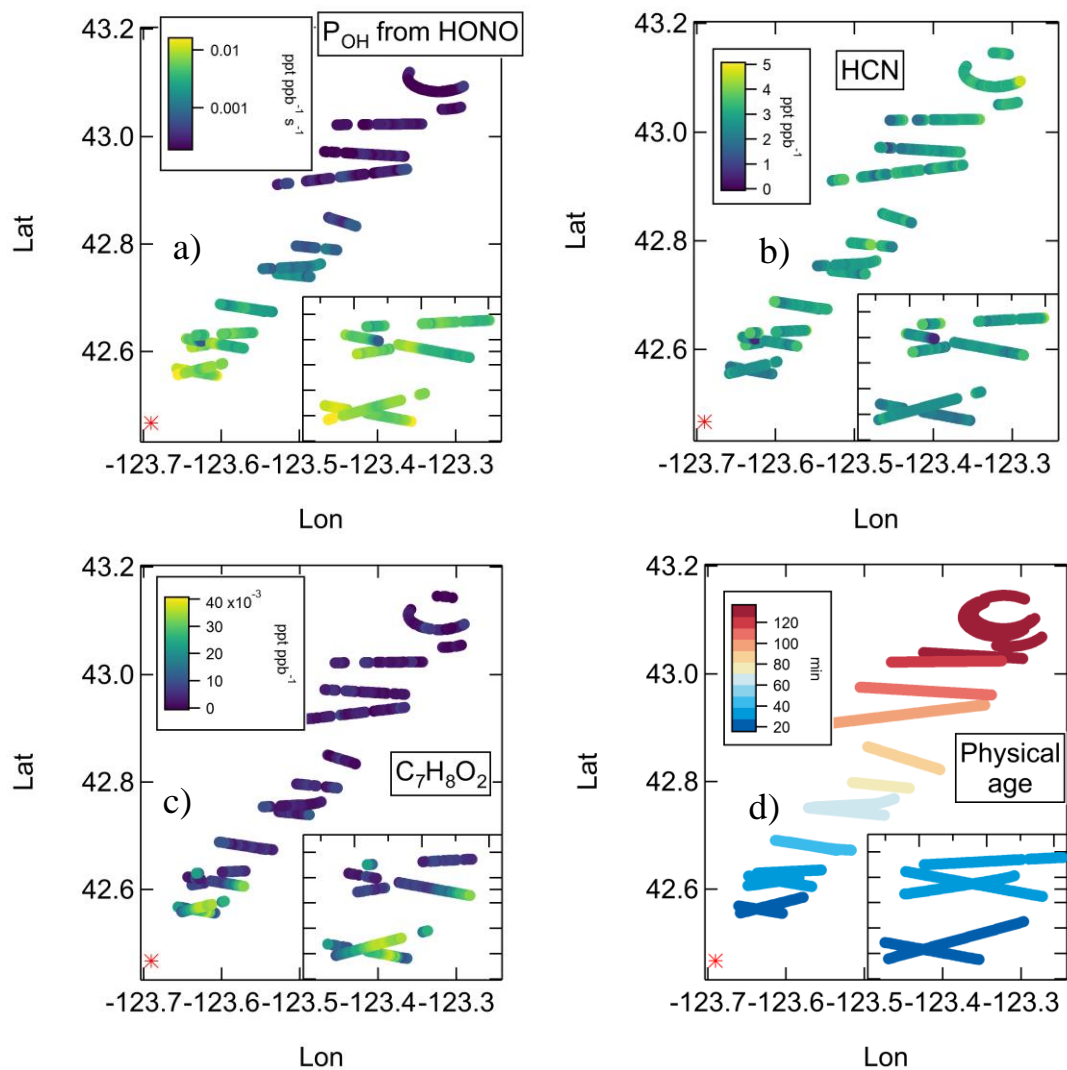
150 Several other vertically stacked transects of the South Sugarloaf fire plume were conducted  
151 in addition to those in Sect. 3.2. In Fig. S10, the upper two crosswind transects through the  
152 plume sampled at an age of 47 min from 1415-1445 LT clearly show steep vertical gradients in  
153 HONO,  $C_6H_6O_2$ , and  $O_3$  at the top of the plume. The uppermost transect appears to have

154 skimmed close to the top of the plume, where photolysis rates were much higher than the other  
155 transect ~350 m lower. In Fig. S11, a stack of transects at the same 47 min age but sampled as  
156 the sun was setting at 1850-1925 LT illustrates how the observed gradients were changing as day  
157 became night. The  $j_{\text{HONO}}$  values were low even outside of the plume, and the horizontal  
158 crosswind gradients in reactive compounds such as HONO and  $\text{C}_6\text{H}_6\text{O}_2$  were much smaller,  
159 indicating OH production and associated chemistry were greatly slowed. In fact,  $\text{O}_3$  was depleted  
160 in all locations inside the plume relative to background air in these evening transects, but  
161 especially in the denser portion of the plume at higher altitudes. Vertical crosswind gradients  
162 were observed for  $\text{O}_3$  and HONO. Some of the horizontal and vertical variability observed for  
163 compounds such as HONO could indicate inhomogeneous emissions or transport across the  
164 plume source, which might be expected with such large fires. The apparent rise in  $\text{C}_6\text{H}_6\text{O}_2$   
165 NEMR as the aircraft exited each transect was likely an artifact caused by the slightly slower  
166 time response for  $\text{C}_6\text{H}_6\text{O}_2$  relative to CO due to interaction with inlet walls in the I CIMS. This  
167 artifact is less apparent in transects sampled during daytime, because the crosswind gradients  
168 from OH chemistry are stronger than the sampling artifact. Fig. S11 illustrates the behavior that  
169 is likely to be observed in wildfire plumes that are emitted at/after sunset. The differences in  
170 observed gradients highlights the need to understand the different chemical and physical  
171 evolution of daytime and nighttime plumes to model the downwind effects of emissions  
172 occurring throughout the day and night.  
173



174  
175  
176  
177  
178  
179  
180  
181

**Figure S1.** Images from the forward facing camera on the C-130 aircraft showing how the Taylor Creek Fire plume injected above the smoke-filled boundary layer into the free troposphere. The image on the left shows the plume shortly after injection, and the image on the right shows the evolution of the plume approximately 90 minutes later.



182

183

184

185

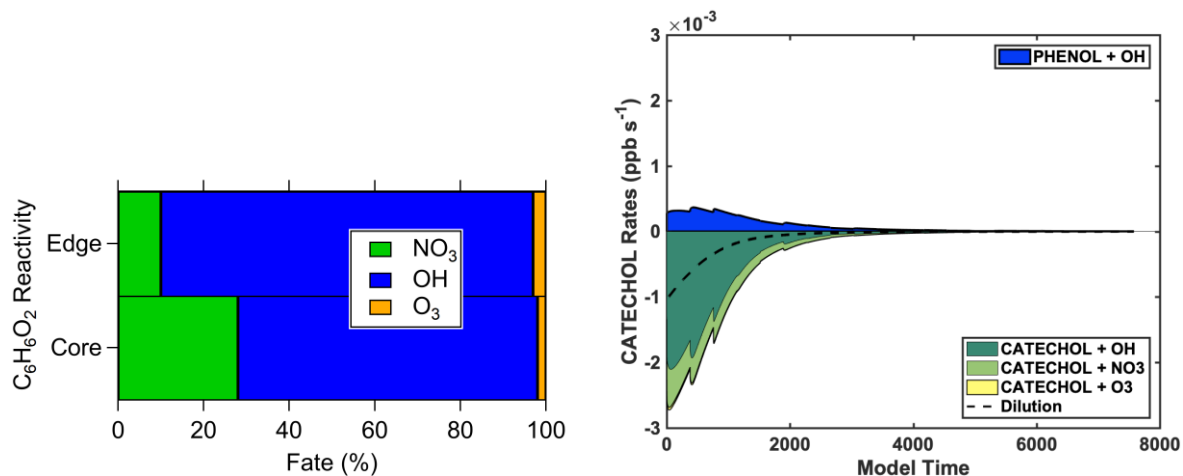
186

187

188

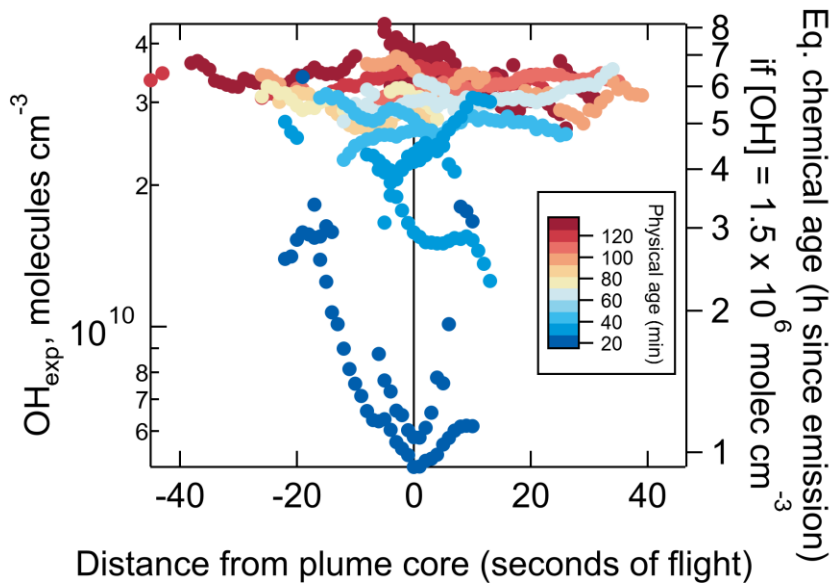
189

**Figure S2.** Plume transects in the Taylor Creek fire, showing spatial variations in a) the dilution-corrected production rate of OH from HONO photolysis, the NEMRs of b) HCN and c)  $C_7H_8O_2$ , and d) the estimated physical age of each transect. The insets show the first five transects in greater detail. Gradients were not observed for HCN, in contrast to the NEMRs of reactive compounds shown in Fig. 1.



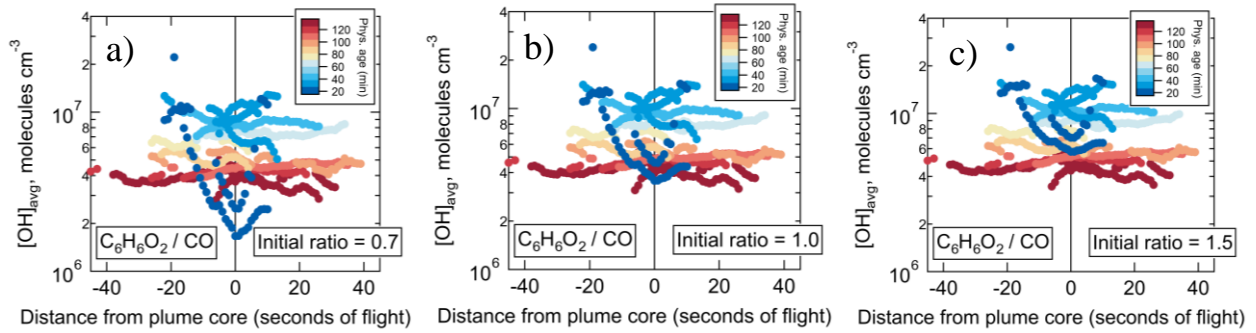
190  
 191 **Figure S3.** Left) Percentage of reactivity of  $C_6H_6O_2$  to oxidants in the Taylor Creek Fire plume  
 192 across entire model run time. The reactivity was modeled using the FOAM box model when  
 193 initializing the model with mixing ratios measured in the plume core (95<sup>th</sup> percentile [CO]) or on  
 194 the plume edges (30<sup>th</sup> percentile values). Right) Production and loss rates of catechol ( $C_6H_6O_2$ ) in  
 195 the plume core as a function of model run time. The fractional fate was roughly constant as a  
 196 function of plume age. The data exhibit a slight sawtooth pattern because photolysis frequencies  
 197 and physical parameters (e.g. temperature and pressure) were manually adjusted at model times  
 198 corresponding to observations at each measured physical age.  
 199





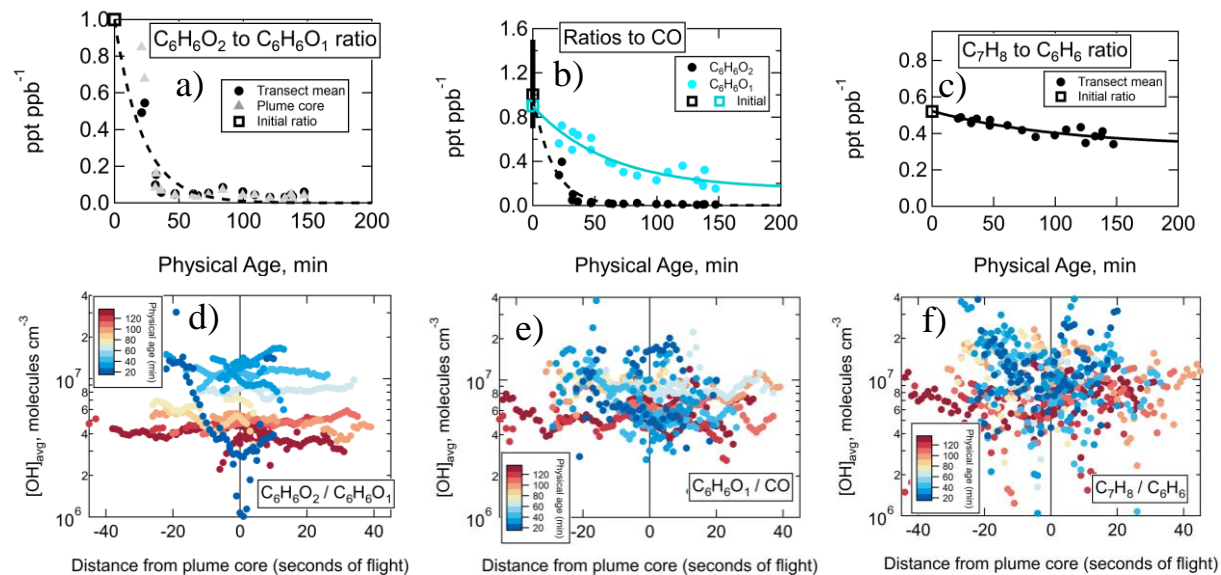
200  
201  
202  
203

**Figure S4.** OH<sub>exp</sub> at each sampled location in the Taylor Creek Fire plume, as a function of distance from the plume core. Data are colored by estimated physical age.



204  
 205  
 206  
 207  
 208  
 209  
 210

**Figure S5.** Calculations of  $[\text{OH}]_{\text{avg}}$  in the Taylor Creek plume using initial  $\text{C}_6\text{H}_6\text{O}_2$  to CO ratios of a) 0.7, b) 1, same as Fig. 2b, and c) 1.5. Data are colored by estimated physical age. This sensitivity analysis illustrates the absolute magnitude of  $[\text{OH}]_{\text{avg}}$  varies by up to a factor of two over this range of initial ratios, but the existence of crosswind gradients and the evolution with plume age is robust.



211

212

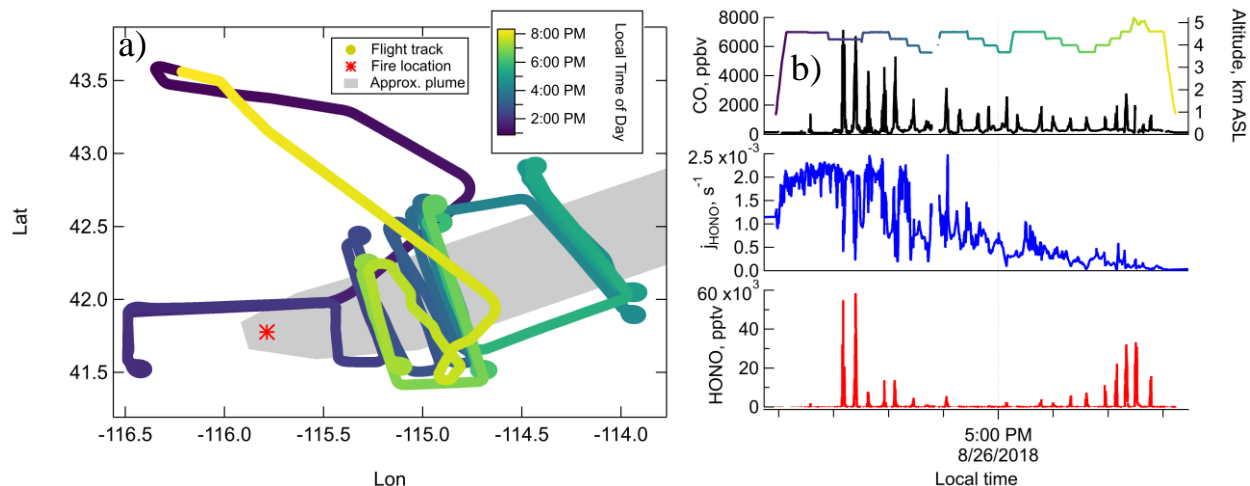
213

214

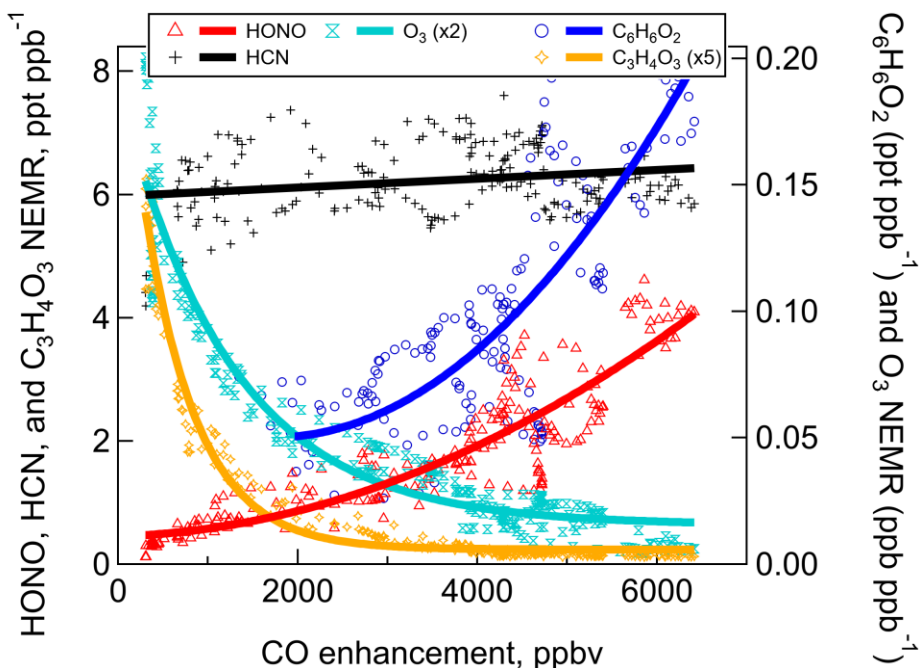
215

216

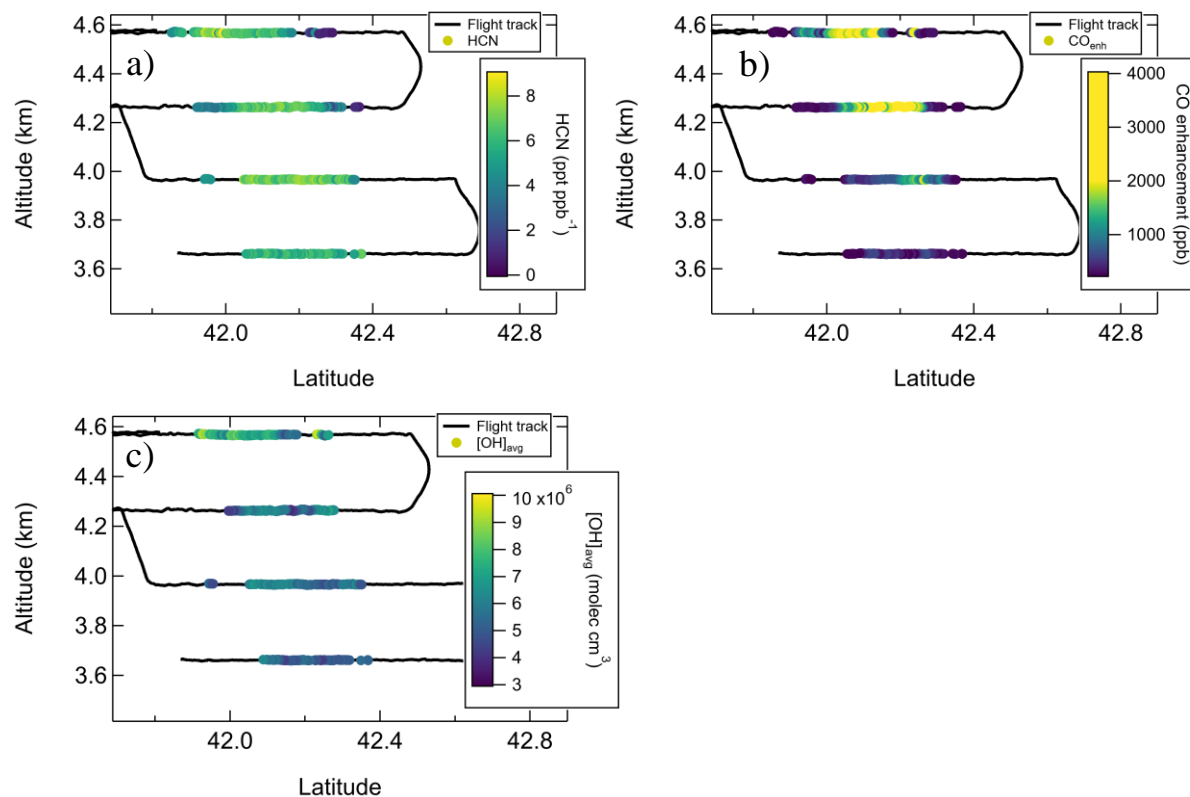
**Figure S6.** a, b, and c) The derivation of initial ratios, and d, e, and f) calculations of  $[OH]_{avg}$  in the Taylor Creek plume using different compound ratios, for comparison to Fig. 2. See Sect. S3 for discussion.



217  
 218 **Figure S7.** a) Flight track for the South Sugarloaf fire on Aug. 26, 2018, colored by local time of  
 219 day and showing approximate fire and plume locations, and b) measurements of altitude, CO,  
 220  $j_{\text{HONO}}$ , and HONO, illustrating the changing photochemical conditions during the time of plume  
 221 sampling. Altitude is also colored by local time of day.  
 222



223  
 224 **Figure S8.** Gradients in several compounds as a function of CO enhancement above background  
 225 in a crosswind transect of the South Sugarloaf fire plume. The highest CO enhancements are near  
 226 the dark plume center, and CO enhancement decreases due to dilution on plume edges. This  
 227 transect was sampled at an est. physical age of 44 min at 1420 LT. Reactive compounds such as  
 228 HONO and  $C_6H_6O_2$  are depleted on plume edges relative to center, due to faster photochemistry.  
 229 Similarly, oxidation products such as  $O_3$  and  $C_3H_4O_3$  are enhanced on plume edges relative to  
 230 center. Not all plume transects have the prototypical Gaussian shape, so plotting as a function of  
 231 CO enhancement instead of distance from plume center (defined by highest CO) can be useful.



232

233

234

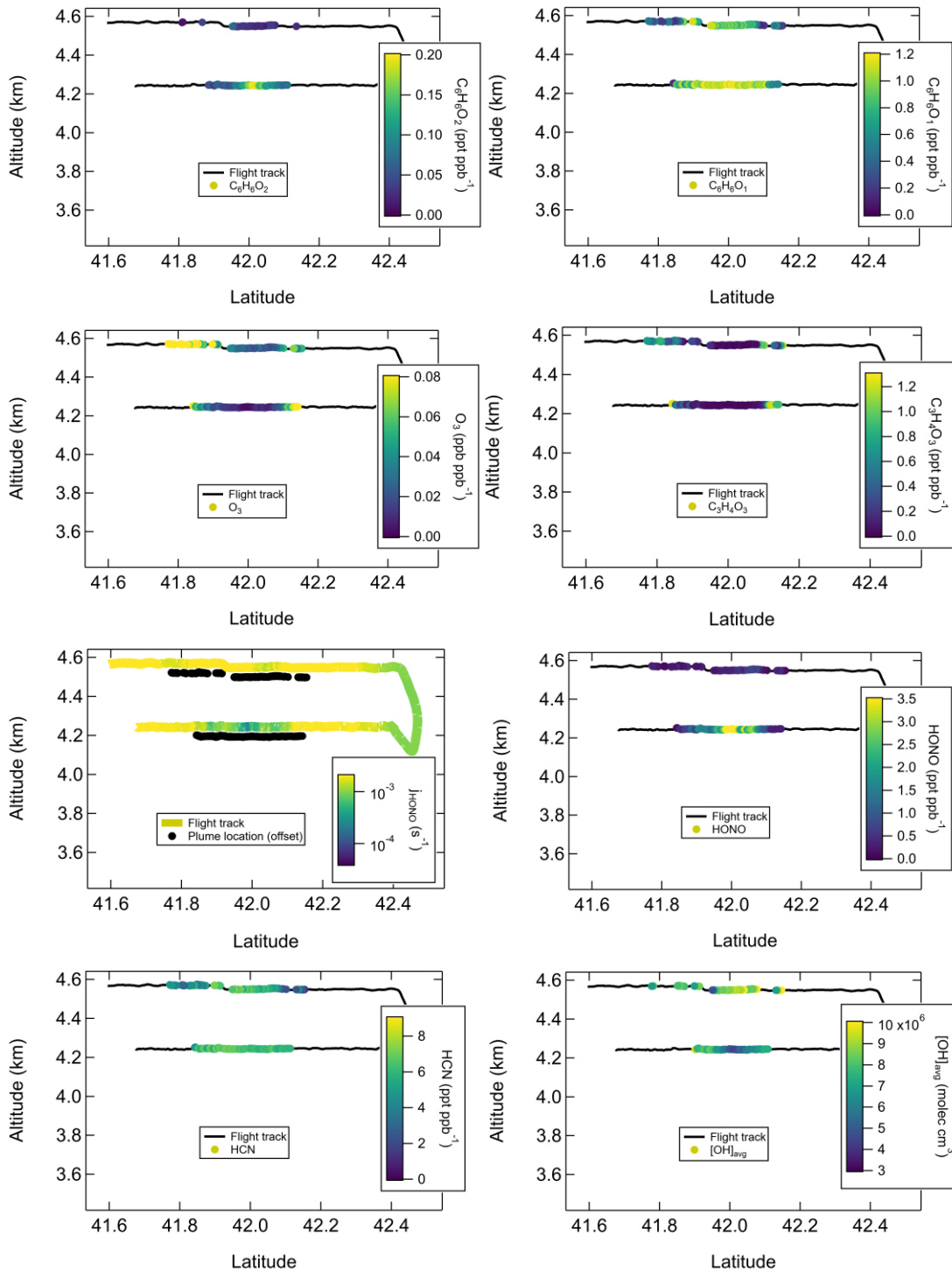
**Figure S9.** For comparison with Fig. 3, a) HCN, b) CO enhancement, and c)  $[OH]_{avg}$  in four vertically stacked transects of the South Sugarloaf fire, sampled at an average est. physical age of 76 min from 1450-1550 LT. Relatively nonreactive compounds such as HCN remain roughly constant throughout each transect.

237

238

239

240



241

242

243

244

245

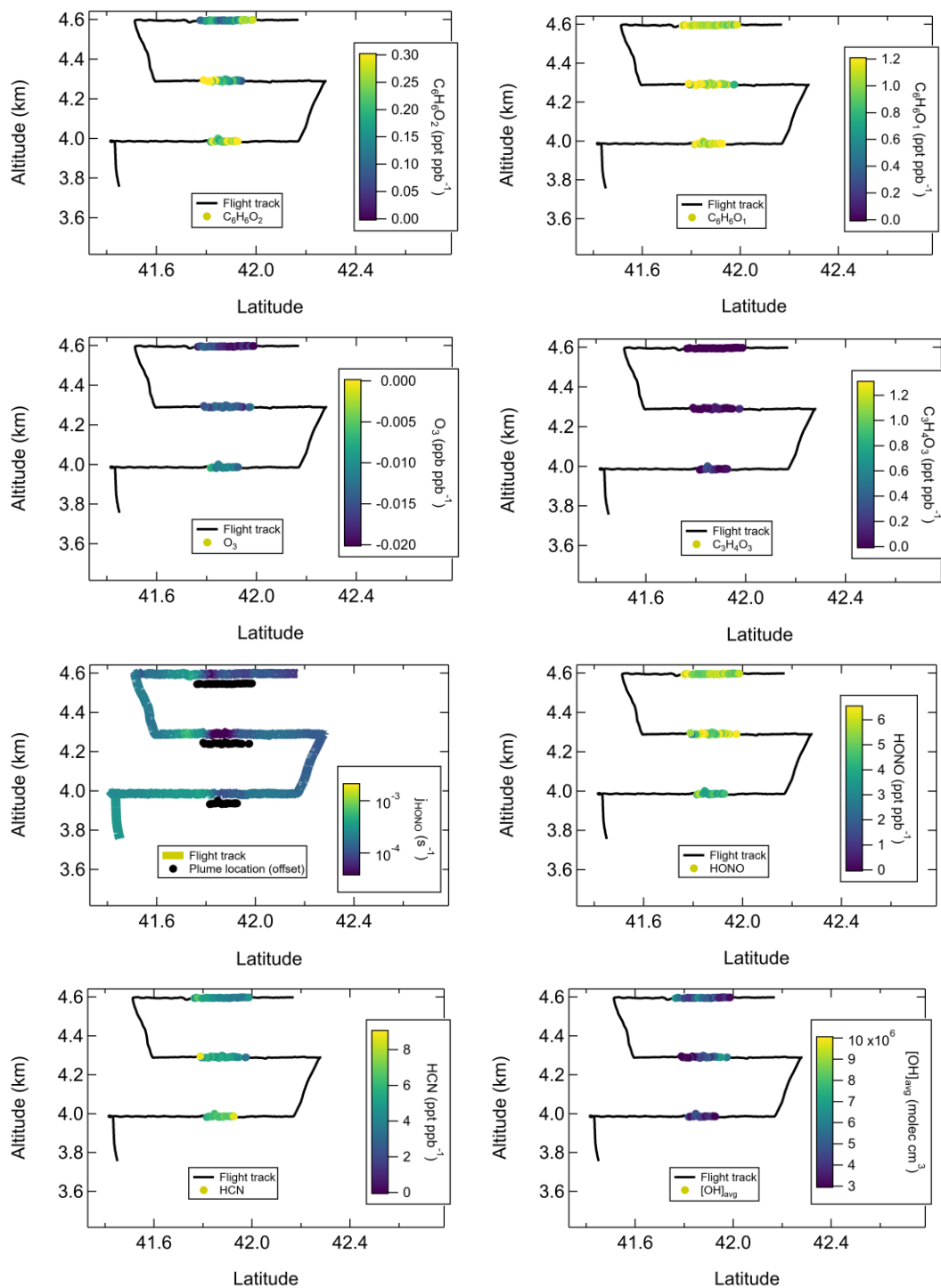
246

247

248

249

**Figure S10.** Various measurements in two vertically stacked transects in the South Sugarloaf fire sampled at an average physical age of 47 min, sampled from 1415-1445 LT. The upper transect had higher photolysis rates, leading to faster  $O_3$  formation with more depleted HONO and  $C_6H_6O_2$ . This figure can be compared with Fig. S11, which shows a similar estimated physical age but sampled late in the day with different chemical conditions leading to weaker gradients.



250

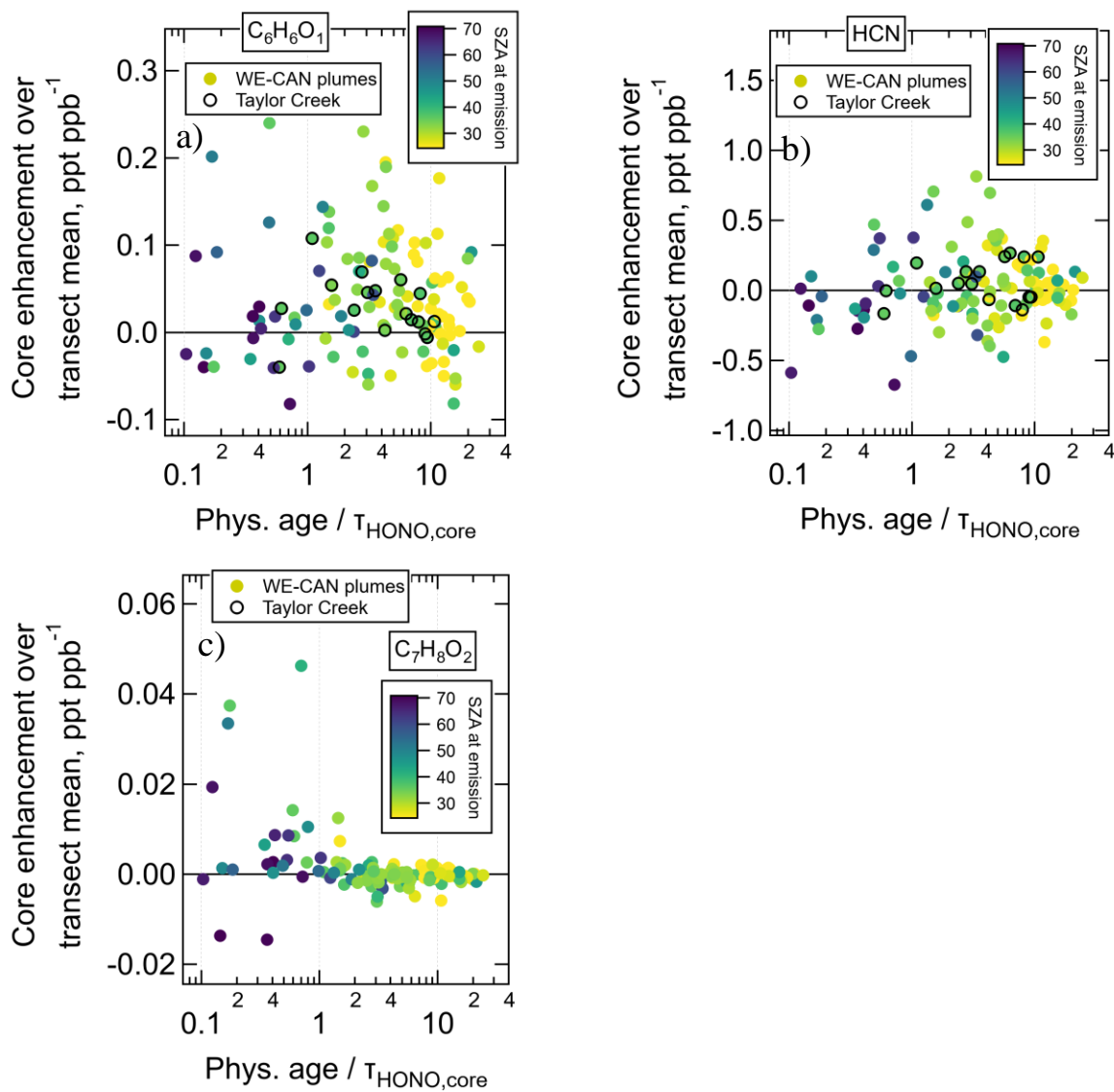
251

252

253

254 **Figure S11.** Various measurements in three vertically stacked transects at an estimated physical age of 47  
 255 min, sampled from 1850-1925 LT, close to sunset.  $O_3$  is depleted relative to the background, with a  
 256 vertical gradient. HONO and  $C_6H_6O_2$  remain in relatively high abundances across the plume transects,  
 257 illustrating slower photochemistry leading to lesser gradients. Horizontal and vertical variability in  
 258 HONO could indicate inhomogeneous emissions/transport across the large fire source, while the  
 259 variability in  $C_6H_6O_2$  is likely due to an inlet sampling artifact (see Sect. S4). This figure can be compared  
 260 with Fig. S10, which shows a similar estimated physical age but sampled in the middle of daytime with  
 261 more rapid chemistry and stronger gradients.





262

263

264

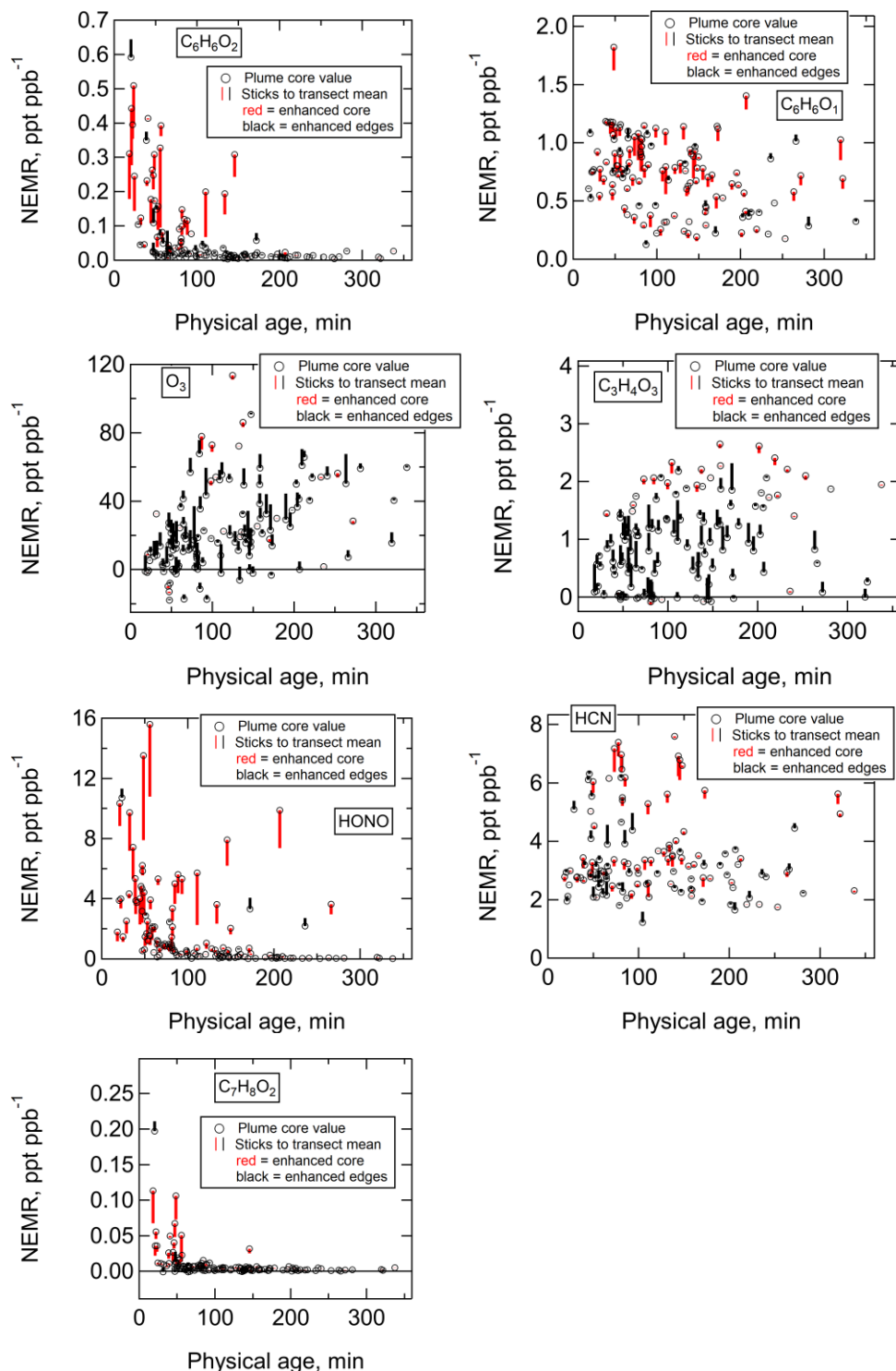
265

266

267

268

**Figure S12.** Enhancements of NEMRs in plume cores (average where [CO] > 90<sup>th</sup> percentile) relative to transect mean NEMRs for all WE-CAN transects, for a)  $C_6H_6O_1$ , b) HCN, and c)  $C_7H_8O_2$  (methyl catechol; see Palm et al., 2020) for comparison with Fig. 4. The Taylor Creek plume transects are highlighted.



269

270

271

272

273

274

275

276

277

278

**Figure S13.** Various NEMR values in the plume cores where [CO] > 90<sup>th</sup> percentile (open circles), relative to transect mean NEMRs (other end of sticks). Sticks are red when the core is higher than the transect mean, and black when the core value is lower. Reactive emissions are generally enhanced in the core, oxidation products are enhanced on the edges, and unreactive compounds such as HCN show little gradients.

279 **Table S1.** Rate constants for reactions of OH with various compounds used in this analysis.

Molecular formula	Compound	k <sub>OH</sub> rate constant (cm <sup>3</sup> molecule <sup>-1</sup> s <sup>-1</sup> )
C <sub>6</sub> H <sub>6</sub> O <sub>1</sub>	Phenol	2.6 x 10 <sup>-11</sup> <sup>(1)</sup>
C <sub>6</sub> H <sub>6</sub> O <sub>2</sub>	Catechol	1.0 x 10 <sup>-10</sup> <sup>(2)</sup>
C <sub>7</sub> H <sub>8</sub>	Toluene	5.6 x 10 <sup>-12</sup> <sup>(3)</sup>
C <sub>6</sub> H <sub>6</sub>	Benzene	1.2 x 10 <sup>-12</sup> <sup>(3)</sup>
CO	Carbon monoxide	2.4 x 10 <sup>-13</sup> <sup>(4)</sup>

280 <sup>1</sup>(Atkinson et al., 1989)281 <sup>2</sup>(Olariu et al., 2000)282 <sup>3</sup>(Atkinson & Arey, 2003)283 <sup>4</sup>(Burkholder et al., 2019)

284